Check for updates

ADVANCED THEORY AND SIMULATIONS
www.advtheorysimul.com

Electronic and Magnetic Properties of The Graphene/RE/Ni(111) (RE: La, Yb) Intercalation-Like Interfaces: A DFT Analysis

Qilin Guo, Roman Ovcharenko, Beate Paulus, Yuriy Dedkov, and Elena Voloshina**

The effect of the rare-earth (RE) metals (La and Yb) intercalation on the electronic and magnetic properties of the graphene/Ni(111) interface is studied using state-of-the-art density functional theory calculations. In both systems, the intercalation of RE leads to the dramatic decrease of the magnetic moments of the Ni-interface atoms and to the negligible moments of C-atoms in a graphene layer, compared to the parent graphene/Ni(111) system. At the same time, the significant *n*-doping of graphene together with a band-gap opening is observed in both cases of the RE intercalation with a position of the graphene Dirac point reaching $E_D - E_F \approx -1.53$ eV. Also the large density of states is found in the vicinity of the Fermi level (E_F) along the $M - K$ direction for the graphene-derived π states which can be attributed to the joint effect of the intercalated RE and interface Ni atoms. These factors – increased density of states at E_F and absence of magnetism of C-atoms in a graphene layer – indicate the possibility of the observation of the superconductive state in graphene in the considered RE-based systems, which is important for the understanding of these and other electronics effects in the graphene-based systems.

1. Introduction

Graphene (gr), a pure 2D layer consisting of carbon atoms arranged in a honeycomb lattice, and different interfaces on its basis play an important role in condensed matter physics and chemistry during last decades.[1–6] In many cases it is caused by the unique physical and chemical properties of a free-standing ideal graphene, which is considered as a model system for the studies of different exciting phenomena. Graphene has an exceptional electronic structure in the vicinity of the Fermi level (E_F), where linearly dispersing energy bands for π electrons form the so-called Dirac cones and point-like Fermi surface. For a graphene layer, which is used or considered in different electronic devices, its electronic spectrum around the Dirac point is usually strongly affected due to the interaction between graphene and contacting material. For example, the adsorption of graphene on ferromagnetic substrates leads to the induced magnetic moment in graphene and the respective spin polarization of the graphene-derived π bands[7–11] as well as to the increased magnetic anisotropy of the underlying magnetic layers.[12,13]

The graphene-based interfaces on metallic or semiconducting supports allow to perform the modification of the electronic and magnetic properties of graphene using either adsorption of different species on top of graphene or intercalation of different materials between graphene and support. Here, in the latter case, the intercalation can lead to the decoupling of graphene from the substrate and restoring the free-standing character of its carriers in the vicinity of E_F. Also, in some cases the intercalation can allow to reach the desired properties of graphene, like the increase of the induced magnetic moment of carbon atoms[8] or to induce the spin-splitting of the graphene-derived bands using intercalated thin layers of heavy metals with strong spin-orbit interaction.[14]

Following the discovery of the superconductivity in the bulk graphite-intercalation compounds (GICs) YbC_6 and CaC_6 with critical temperatures of 6.5 and 11.5 K, respectively,[15–17] the superconducting state was later confirmed for the Ca-doped graphene laminates and graphene bi-layers (C_6CaC_6) with a critical temperature of $\approx 4 - 6$ K and ≈ 2 K, respectively.[18,19] Further

Q. Guo, Y. Dedkov, E. Voloshina
Department of Physics
Shanghai University
Shangda Road 99, Shanghai 200444, China
E-mail: dedkov@shu.edu.cn; voloshina@shu.edu.cn
R. Ovcharenko
Max-Born-Institut für Nichtlineare Optik und Kurzzeitspektroskopie
Max-Born-Straße 2A, Berlin 12489, Germany
B. Paulus, E. Voloshina
Institut für Chemie und Biochemie
Freie Universität Berlin
Arnimallee 22, Berlin 14195, Germany
Y. Dedkov, E. Voloshina
Centre of Excellence ENSEMBLE3 Sp.z o. o.
Wolczynska Str. 133, Warsaw 01-919, Poland

The ORCID identification number(s) for the author(s) of this article can be found under https://doi.org/10.1002/adts.202100621

© 2022 The Authors. Advanced Theory and Simulations published by Wiley-VCH GmbH. This is an open access article under the terms of the Creative Commons Attribution-NonCommercial-NoDerivs License, which permits use and distribution in any medium, provided the original work is properly cited, the use is non-commercial and no modifications or adaptations are made.

DOI: 10.1002/adts.202100621

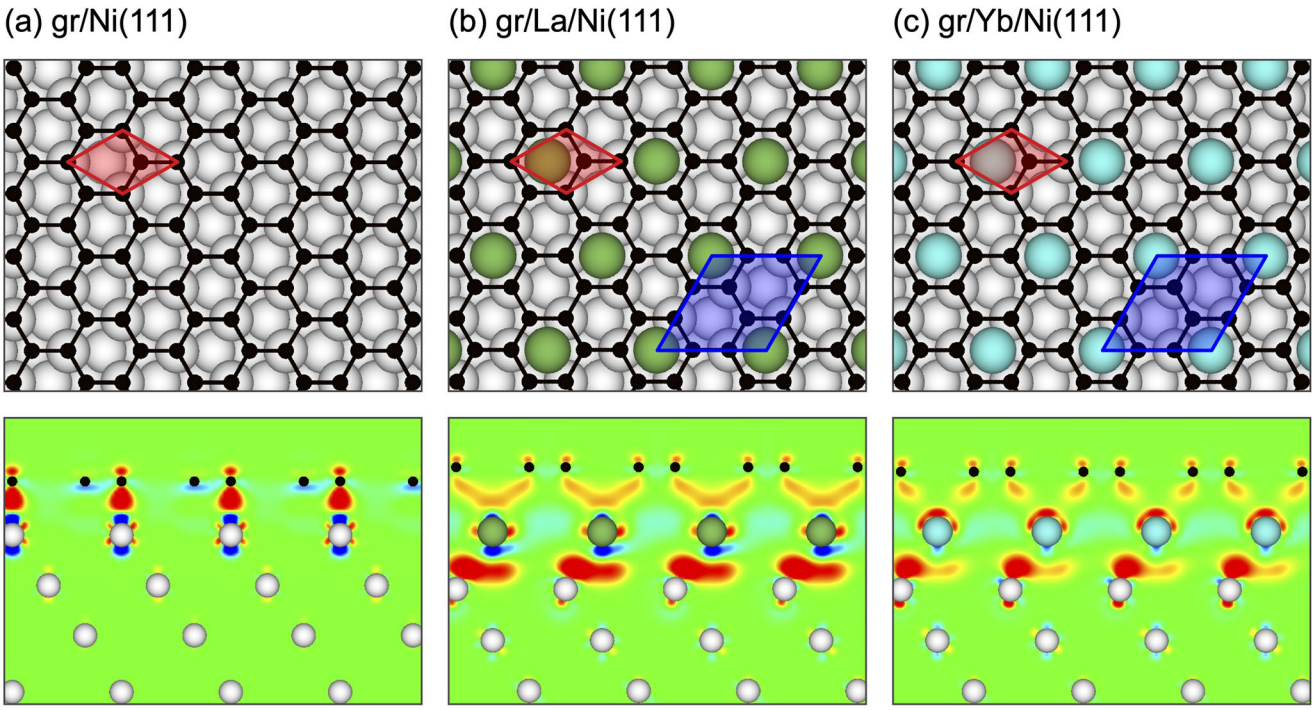

Figure 1. Top and side views of a) gr/Ni(111), b) gr/La/Ni(111), and c) gr/Yb/Ni(111). Black, green, turquoise, and white spheres are C, La, Yb, and Ni atoms, respectively. Small (red) and large (blue) rhombus indicate unit cells of graphene/Ni(111) and gr/RE/Ni(111), respectively. Side views for all structures are taken along the graphene arm-chair edge and they are overlaid with electron charge difference maps: $\Delta\rho(\mathbf{r}) = \rho_{\mathrm{gr/RE/Ni}}(\mathbf{r}) - [\rho_{\mathrm{gr}}(\mathbf{r}) + \rho_{\mathrm{RE}}(\mathbf{r}) + \rho_{\mathrm{Ni}}(\mathbf{r})]$. Here, $\Delta\rho(\mathbf{r})$ is color coded as blue ($-0.01\,e$ Å^{-3}) – green (0) – red ($+0.01\,e$ Å^{-3}).

systematic experimental and theoretical studies of these systems show that huge n-doping of graphene layers leads to the shift of E_F reaching the van Hove singularity formed by the π^* band along the $K-M$ direction of the Brillouin zone. This increase of the density of states in the vicinity of E_F also leads to the enhancement of the electronic correlations as well as of the electron–phonon coupling in the graphene-based systems.[16,17,20,21] Further spectroscopic experiments performed on the metal supported graphene layers and intercalated with alkali- and alkali-earth metals indicated very strong electron–phonon coupling for the case of Ca-intercalated graphene with predicted transition temperature of 1.5 K,[22] which, however is not yet experimentally confirmed. Considering the similarity between bulk YbC_6 and CaC_6, further spectroscopic experiments were also devoted to the Yb-intercalated graphene-based system gr/Yb/SiC(0001),[23,24] where a strong shift of the graphene-derived bands was observed and in the overdoping regime the electronic bands renormalization along the $K-M$ direction was observed.

Graphene intercalation-like systems with different rare-earth (RE) metals as intercalants were intensively studied in the past.[25–31] However, the theoretical analysis of the electronic and magnetic properties of the gr/RE/metal interfaces is rarely addressed. Here, we present the systematic state-of-the-art density functional theory (DFT) studies of the gr/RE/Ni(111) interface with La and Yb as intercalants. These elements present two limited cases of the tri- and divalent metals with empty and fully occupied 4f orbitals for La ($6s^25d^14f^0$) and Yb ($6s^25d^04f^{14}$), respectively. Both intercalation systems are considered in the most stable geometry, where RE atoms form the $(\sqrt{3}\times\sqrt{3})R30°$ structure with respect to the parent gr/Ni(111) system. Our DFT results show very high *n*-doping of graphene with restoring of the linear dispersion of the graphene-derived π band in the vicinity of the Dirac point, reaching the position $E_D - E_F \approx -1.53$ eV. At the same time a sizeable band gap is opened at the Dirac point for the graphene π band, attributed to the broken sublattice symmetry in a graphene layer and to the respective hybridization of the valence band states of graphene and RE. The observed huge doping level of graphene in both gr/RE/Ni(111) systems leads to the increased density of states at E_F arising from the van Hove singularity of the graphene states. This effect is attributed to the joint electron doping induced by RE and interface Ni atoms. These results indicate the possibility to observe the superconductive state for a graphene layer in the considered systems.

2. Results and Discussion

Figure 1 shows top and side views of the studied systems: (a) parent gr/Ni(111) interface and (b) gr/La/ Ni(1111), (c) gr/Yb/Ni(111) intercalation-like interfaces. The widely accepted structure of gr/Ni(111) is when carbon atoms are arranged in the so-called *top-fcc* configuration on Ni(111).[32–35] In this case, one of the carbon atoms of the graphene unit cell is placed above the top Ni atom and the second carbon atom is placed in the *fcc* hollow site of Ni(111) slab (Figure 1a). Our present calculations confirmed this model (see Table S1 and Figure S1, Supporting Information). The small distance of 2.11 Å between a graphene layer and Ni(111) leads to the effective overlapping of the valence band states at the interface causing the appearance

© 2022 The Authors. Advanced Theory and Simulations published by Wiley-VCH GmbH

Table 1. Results for the atomic structure of the studied gr/metal interface: E_{int} (in meV per C-atom) is the interaction energy, defined as $E_{int} = E_{gr/s} - (E_{gr} + E_s)$, where $E_{gr/s}$ is the total energy of the graphene/substrate system, and E_{gr} and E_s are the energies of the fragments at the same coordinates as in the graphene/substrate system; d_0 (in Å) is the mean distance between the graphene overlayer and the interface metal layer; d_1 (in Å) is the mean distance between the interface metal layer and the second metal layer; d_2 (in Å) is the mean distance between the second and third metal layers; m_C (in μ_B) is the interface carbon spin magnetic moment (several values for the nonequivalent carbon atoms are indicated); m_{Ni} (in μ_B) is the interface nickel spin magnetic moment; m_{RE} (in μ_B) is the RE spin magnetic moment; $E_D - E_F$ (in eV) is the position of the Dirac point with respect to the Fermi energy (two values are given for the spin-up and spin-down channels, respectively); E_g (in meV) is the band gap at the Dirac point (two values are given for the spin-up and spin-down channels, respectively).

System	Graphene/Ni(111)	Graphene/La/Ni(111)	Graphene/Yb/Ni(111)
E_{int}	−165	−170	−156
d_0	2.11	2.54	2.35
d_1	1.99	2.26	2.30
d_2	1.97	2.02	2.00
m_C	−0.018/0.030	0.002/0.004	0.000/0.002
m_{Ni}	0.513	0.319	0.440
m_{RE}		−0.022	−0.003
$E_D - E_F$		−1.410/ − 1.350	−1.535/ − 1.525
E_g		320/220	250/230

of the effective magnetic moment of carbon atoms that was confirmed in the experiment (Figure 1a, **Table 1**).[7,8,36]

Considering the formation of the La- and Yb-based gr/RE/Ni(111) interfaces it is assumed that RE atoms form the $(\sqrt{3} \times \sqrt{3})R30°$ structure with respect to the parent gr/Ni(111) interface as it was experimentally found for the bulk and surface La- and Yb-GICs[37–39] as well as for the discussed graphene–Ni-based interfaces.[25,27] The sharp interfaces between all components are considered taking into account the annealing temperature of 250 – 300° C needed for the intercalation of RE in gr/Ni(111) and gr/SiC(0001).[23,27] Taking into consideration the possible crystallographic structures of the obtained RE-intercalation-like systems, one can see that the atoms of intercalant can be placed either in the FCC or in the HCP hollow sites of the Ni(111) slab or above the interfacial (TOP) nickel atom. Our calculations demonstrate that the *top-fcc*_HCP arrangement (where *top-fcc* stands for the arrangement of carbon atoms above Ni(111)) is significantly more stable from the energetic point of view (see Table S1 and Figure S2, Supporting Information). This result is similar to the previously published data for the gr/Eu/Ni(111) system.[30] The top and side views of the relaxed gr/RE/Ni(111) structures are shown in Figure 1b,c. The distance between the graphene layer and the underlying RE and the corresponding interaction energies between graphene and substrate (Table 1) place gr/RE/Ni(111) (RE: La, Yb) between "strongly" and "weakly" interacting graphene–metal systems.[40,41]

Analysis of the electron charge difference maps for the gr/RE/Ni(111) systems presented for side views in Figure 1 indicates the strong charge redistribution in the intercalation-like systems. For the parent gr/Ni(111) system the orbital overlap for the valence band states of graphene and Ni leads to the formation of the hybrid states at the gr–Ni interface. The inclusion of RE atoms at the interface leads to the enhanced electron density accumulation on graphene layer leading to the strong *n*-doping of graphene. The electron density on graphene and at the gr–La interface is slightly larger compared to the case of the gr–Yb interface that can be due to the trivalent electronic configuration of La ($6s^2 5d^1 4f^0$) compared to the divalent electronic configuration of Yb ($6s^2 5d^0 4f^{14}$). Also the effect of hybridization of the graphene π and La 5d states can be visible from the electron charge difference map for gr/La/Ni(111). The strong charge transfer from RE atoms on graphene is compensated by the respective electron transfer from the underlying Ni layer on RE atoms, which is larger in the case of La, compared to Yb, due to the larger electron transfer for the gr–La interface.

Figure 2 shows the calculated spin-resolved band structures and respective density of states (DOS) plots for all considered systems: (a) gr/Ni(111), (b) gr/La/Ni(111), and (c) gr/Yb/Ni(111). (The corresponding band structure plots in a wider energy range are presented in Figure S3–S5, Supporting Information, respectively.) The modification of the electronic structure of graphene upon its adsorption on ferromagnetic Ni(111) was discussed earlier in a series of experimental and theoretical works,[9,33,35,40] which identify the significant changes in the electronic structure of graphene in this system compared to free-standing graphene: graphene is strongly *n*-doped; formation of $\pi - d$ hybrid states yields a massive rearrangement of bands (Figure 2a and Figure S3, Supporting Information); magnetic moments on carbon atoms are induced (Table 1).

The intercalation of RE atoms in gr/Ni(111) interface leads to the decoupling of the electronic states of graphene and substrate and partial restoring of the linear dispersion of the graphene-derived π band in the vicinity of the Dirac point (Figure 2b,c). At the same time, due to the partial transfer of the mobile valence band electrons of RE on the π^* state of graphene, the strong *n*-doping of graphene is observed for both gr/RE/Ni(111) systems, with a position of a Dirac point of graphene well below E_F. This shift of the Dirac point amounts to $E_D - E_F \approx -1.38$ eV and $E_D - E_F \approx -1.53$ eV for the La- and Yb-intercalation-like systems, respectively (Figure 2b,c). As can be seen from the calculated band structures, the sizeable band gap of ≈ 0.3 eV and ≈ 0.2 eV is open in the electronic spectrum of the graphene-derived π electrons directly at the Dirac point for gr/La/Ni(111) and gr/Yb/Ni(111), respectively, that is due to the broken sublattice symmetry for carbon atoms of the graphene lattice and because of the effect of hybridization between valence band states of graphene and underlying RE metal. However, in both cases such effect of hybridization is observed for the valence band states of RE well away from the Dirac point. The inclusion of the spin-orbit interaction for the Yb 4f electrons splits this level into two components and additional energy gaps appear for the graphene-derived π bands due to the avoided-crossing mechanism with flat Yb 4f bands (see Figure S6, Supporting Information). However, the size of the band gap at the *K* point for the π band remains almost the same, ≈ 240 meV.

The effect of decoupling of the valence band states of graphene and Ni(111) as well as the absence of the strong hybridization between states of graphene and RE is nicely detected by the binding

© 2022 The Authors. Advanced Theory and Simulations published by Wiley-VCH GmbH

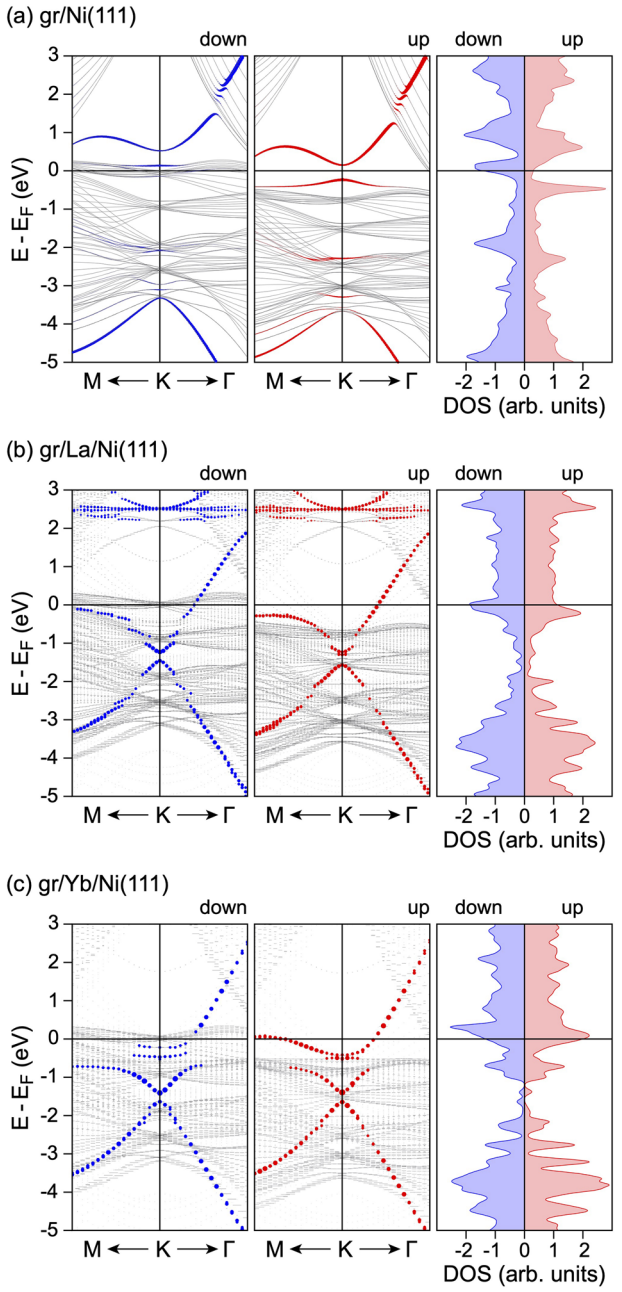

Figure 2. Band structures and C-p_z projected density of states calculated for a) gr/Ni(111), b) gr/La/Ni(111), and c) gr/Yb/Ni(111). The weight of the C-p_z states in the band structures is proportional to the width of the colored line.

energy of the graphene π band at the Γ point (see Figure 2a–c and Figures S3–S5, Supporting Information). The initial binding energy for this band in gr/Ni(111) is ≈ −9.8 eV, which is in quite good agreement with the available experimental data.[7,9] As was discussed earlier, this large binding energy is caused by two effects–electron transfer from Ni to graphene as well as by the strong hybridization of the valence band state of Ni and graphene, that "pushes" graphene-derived π bands to the large binding energies. Here, one can also note the different binding energy change for the graphene-derived π and σ states in comparison with the free-standing graphene, supporting this consideration (Figure S3, Supporting Information). The intercalation of RE metals in gr/Ni(111) keeps the large electron transfer and graphene remains strongly *n*-doped. However, the absence of the strong hybridization of the valence band states of graphene and RE reduces the binding energy of the graphene-derived π band and the difference for the binding energy for the π and σ bands in comparison with those for the free-standing graphene becomes the same (Figures S4 and S5, Supporting Information). The obtained reduction of the binding energy of the π band upon the intercalation of La and Yb in gr/Ni(111) is partially supported by the experimental data where the similar effect (although smaller) was observed.[27]

The most important fact is the observation of the increased graphene-derived π density of states at E_F for both intercalation-like systems, gr/La/Ni(111) and gr/Yb/Ni(111) (Figure 2b,c; Figures S4, S5, Supporting Information). As can be seen from the comparison of the DOS plots with calculated band structures, this increased density of states originates from the almost flat band located in the vicinity of E_F along the $K-M$ direction of the Brillouin zone. Its existence around E_F can be assigned to the joint effect of RE and interface Ni atoms which donate enough electrons to place this band to low binding energy. Our analysis shows that both inequivalent C-atoms contribute equally to the discussed energy band. Taking into account that the hybridization of the valence band states of graphene and RE is small (if any) we can suggest that the appearance of this band in the studied RE-intercalation-like systems might lead to the existence of the superconductive state of graphene in these systems. Such possibility is also supported by the absence of any sizeable magnetic moment of C-atoms in the gr/RE/Ni(111) systems. The intercalation of RE atoms leads to the strong reduction of magnetic moment of the interface Ni atoms from 0.513 μ_B for gr/Ni(111) to 0.319 μ_B and 0.440 μ_B for gr/La/Ni(111) and gr/Yb/Ni(111), respectively. The induced magnetic moments of intercalated RE atoms are relatively small and antiparallel to magnetic moments of interface Ni atoms (see Table 1), because the induced magnetism in La (empty 4f orbitals) and Yb (fully occupied 4f orbitals) is governed by mobile valence 6s electrons, which are ferromagnetically coupled to mobile Ni 4s electrons with magnetic moments antiparallel to Ni 3d electrons, which are mainly responsible for magnetic moments of Ni atoms.[8,42]

In order to make a link to the future experimental data, the scanning tunneling microscopy (STM) images and C *K* near-edge X-ray absorption fine structure spectra (NEXAFS) were calculated for all considered systems. **Figure 3** shows a compilation of STM images for the considered gr/RE/Ni(111) intercalation-like systems calculated for bias voltages corresponding to occupied (upper row) and unoccupied (bottom row) valence band states, respectively. The calculated images for the parent gr/Ni(111) interface are in very good agreement with previously published experimental and theoretical data,[9,30,41,43–45] which clearly indicate the broken sublattice symmetry in the graphene layer adsorbed on Ni(111) and where bright spots in STM images correspond to the C-top atoms. The intercalation of La or Yb atoms in gr/Ni(111) changes significantly the electronic structure of the interface with large electron density located on the interfaced RE atoms. As a consequence of this, the

© 2022 The Authors. Advanced Theory and Simulations published by Wiley-VCH GmbH

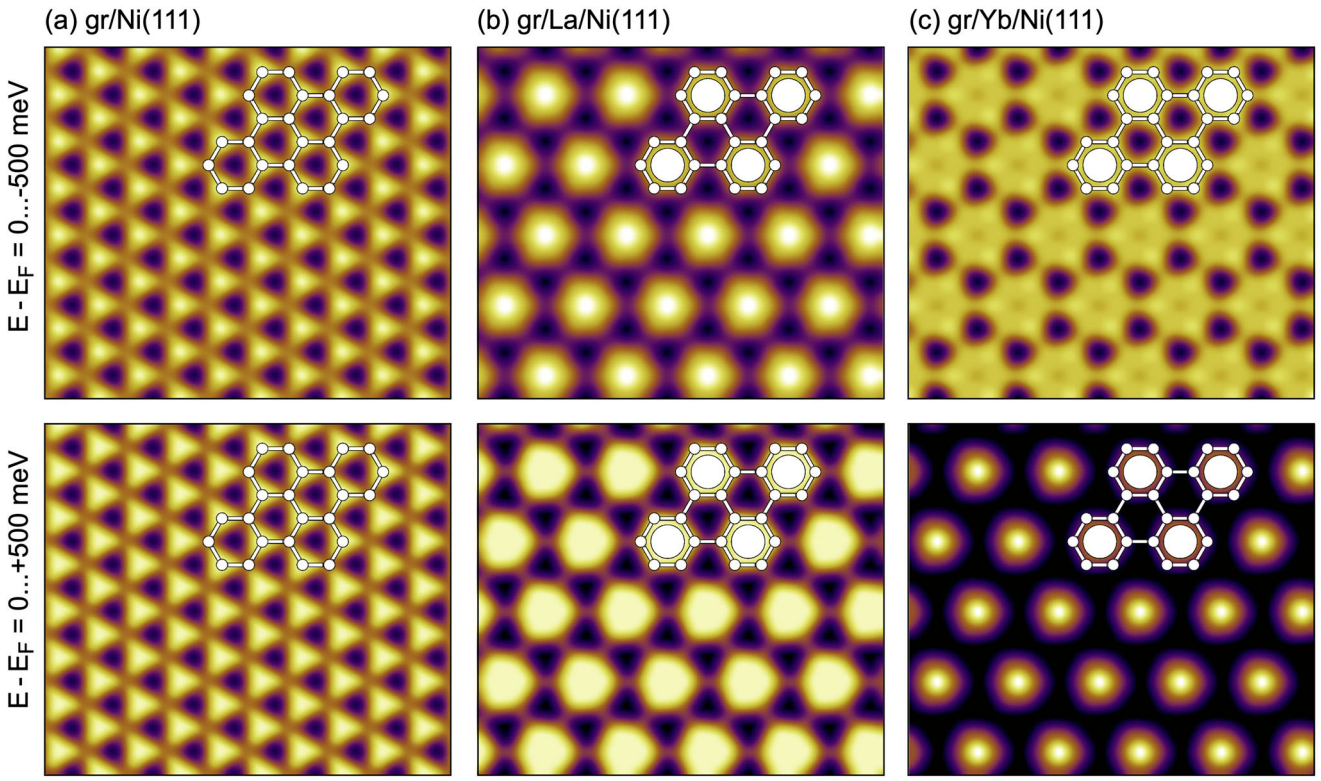

Figure 3. Simulated STM images of a) gr/Ni(111), b) gr/La/Ni(111), and c) gr/Yb/Ni(111), respectively, for occupied ($E - E_F = -500$ meV) (top row) and unoccupied ($E - E_F = +500$ meV) states (bottom row). The images correspond to a tunneling current of 1 nA.[63] The STM pictures are overlaid with the crystallographic structures of the studied system (Ni atoms are not shown).

STM imaging contrast for gr/RE/Ni(111) systems is defined by the $(\sqrt{3} \times \sqrt{3})R30°$ structure of these interfaces with bright spots at the positions of the RE atoms. The modulation of the imaging contrast due to the presence of the graphene lattice is also visible, however its contribution is small, which is in good agreement with previous theoretical results for gr/Eu/Ni(111)[30] and can be compared (to some extent) with the available experimental STM data for La-GIC.[46]

Figure 4 shows a series of the calculated C *K*-edge NEXAFS spectra for graphene, gr/Ni(111) and gr/RE/Ni(111). The method of NEXAFS spectroscopy is used to study the electronic structure of the unoccupied valence band states above E_F and it is a complementary method to X-ray photoelectron spectroscopy and angle-resolved photoelectron spectroscopy used for the investigation of the energy distribution of the occupied states. In the considered NEXAFS spectra the core-level 1s electron of the carbon atom in a graphene layer is excited on the unoccupied valence band states above E_F and being the atomic- and orbital-selective it allows to get information about the energy distribution of the π^* and σ^* states in a graphene layer. In the simulated NEXAFS spectra the region of $-2 \ldots 4$ eV of the relative photon energy corresponds to the $1s \rightarrow \pi^*$ transitions, with higher energy region above 5 eV corresponding to the $1s \rightarrow \sigma^*$ transitions.[47–50] (The peak at 8 eV is possibly due to the quickly completely screened initial state density of states.)

After graphene adsorption on Ni(111) the C *K* NEXAFS spectrum is strongly modified (Figure 4). First, the $1s \rightarrow \pi^*$ peak is split in two components with the second peak placed ≈ 2 eV at higher energies and it corresponds to the respective predominant contributions of two different carbon atoms in gr/Ni(111) to the corresponding unoccupied valence states above E_F. Also the energy difference between $1s \rightarrow \pi^*$ and $1s \rightarrow \sigma^*$ transitions is reduced due to the partial sp^2 rehybridization in a graphene layer adsorbed on Ni(111).[7,9,49,50]

As was shown earlier, the intercalation of La and Yb in gr/Ni(111) leads to the decoupling of a graphene layer from substrate and to the restoring of a "free-standing" character of its electronic states accompanied by heavy *n*-doping. It is immediately reflected in the corresponding NEXAFS spectra of the gr/RE/ Ni(111) intercalation-like systems (Figure 4). In case of gr/Yb/Ni(111), the C *K*-edge NEXAFS spectrum is similar to the one for free-standing graphene: sharp peak corresponding to the $1s \rightarrow \pi^*$ transition and the distance between $1s \rightarrow \pi^*$ and $1s \rightarrow \sigma^*$ peaks is restored to the value of ≈ 6.5 eV. The weak interaction between valence band states of graphene and underlying Yb layer does not lead to strong modifications of the corresponding NEXAFS spectrum.

In case of the gr/La/Ni(111) system, the situation is similar to the one of Yb-intercalation: decoupling of the graphene layer leads to the restoring of the $1s \rightarrow \pi^*$ and $1s \rightarrow \sigma^*$ peaks energy difference which can be taken as an indicator. However, in the present case a new strong peak is observed at ≈ 2.5 eV in the NEXAFS energy region corresponding to the $1s \rightarrow \pi^*$ transition. The analysis of the electron charge difference map for gr/La/Ni(111) (Figure 1b) and the corresponding band structure (Figure 2b and Figure S4, Supporting Information) allows to

© 2022 The Authors. Advanced Theory and Simulations published by Wiley-VCH GmbH

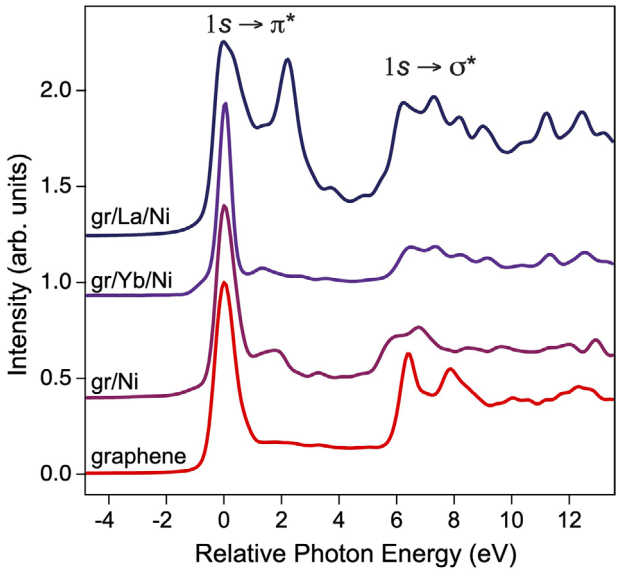

Figure 4. Calculated C *K* NEXAFS spectra for $\alpha = 40°$ for graphene, gr/Ni(111), gr/La/Ni(111), and gr/Yb/Ni(111) (α is an angle between electric field vector of X-ray and the normal to the surface). The position of the first peak of the 1s → π^* transition was set to zero relative photon energy for all spectra, which were also shifted in the vertical direction for clarity.

conclude that this strong peak is a result of hybridization of the unoccupied graphene π^* and La 4f states (with small admixture of the 5d states). These results are in very good agreement with the available experimental data for the La-GIC system, where double-peak structure was observed in the C *K* NEXAFS spectra[51] and previously was assigned to the graphene π^* - La 5d orbitals hybridization. It is interesting to note that in the NEXAFS spectra for both gr/RE/Ni(111) system one can clearly resolve the small shoulder at the low energy side of the 1s → π^* peak, which can be assigned to the increased density of states at E_F due to the strongly shifted π-band along the $K - M$ direction of the Brillouin zone.

3. Conclusions

Using state-of-the-art DFT calculations the electronic properties of different systems obtained via intercalation of La and Yb in gr/Ni(111) were studied. It is found that RE metals-intercalation leads to the restoring of the linear dispersion of the graphene π bands together with a strong *n*-doping of a graphene layer with a position of the Dirac point reaching ≈ -1.53 eV below E_F. Such shift of the electronic bands of graphene leads to the appearing of the π states in the vicinity of the Fermi level along the $K - M$ direction with the respective formation of the van Hove singularity in the density of states distribution. The strong doping can be attributed to the joint effect of RE and Ni atoms at the gr-metal interface. The observed behavior of the graphene electronic bands together with the quenched magnetic moment of the underlying RE and Ni atoms could lead to the superconductivity of graphene in the considered systems. As a link to the future experimental studies of the gr/RE/Ni(111) systems, the STM images and NEXAFS spectra are calculated, which allow to clearly identify the spectroscopic and microscopic properties of the formed systems. The obtained results are of importance for the studies of different graphene-based intercalation-like systems, where different fascinating phenomena can be observed, like for example, low-dimensional superconductivity, electron localizations, different spin configurations.

4. Experimental Section

Spin-polarized DFT calculations based on plane-wave basis sets of 500 eV cutoff energy were performed with the Vienna ab initio simulation package.[52–54] The Perdew–Burke–Ernzerhof exchange-correlation functional[55] was employed. The electron–ion interaction was described within the projector augmented wave method[56] with C (2s, 2p), Ni (3d, 4s), La (4f, 5s, 5p, 5d, 6s), and Yb (4f, 5s, 5p, 6s) states treated as valence states. The Brillouin-zone integration was performed on Γ-centered symmetry reduced Monkhorst–Pack meshes using a Methfessel–Paxton smearing of first order with $\sigma = 0.15$ eV, except for the calculation of total energies and densities of states (DOSs). For those calculations, the tetrahedron method with Blöchl corrections[57] was employed. A $12 \times 12 \times 1$ *k*-mesh was used. Dispersion interactions were considered by means of DFT-D3 correction method of Grimme et al.[58] The DFT+*U* scheme[59] was adopted for the treatment of Yb 4f orbitals, with the parameters $U = 2.0$ eV and $J = 0.7$ eV.[21] The studied systems were modeled using supercells, which have a $(\sqrt{3} \times \sqrt{3})R30°$ overstructure with respect to the unit cell of graphene (Figure 1b,c) and consisted of 53 atoms: 13 layers of nickel atoms (three atoms per layer) with one La or Yb layer (one atom each) and a graphene sheet (six atoms per layer) adsorbed on both sides of the slab. In order to prevent inter-layer interaction within the periodic images, a vacuum spacing of 20 Å was applied for all systems. The lattice constant in the lateral plane was set according to the optimized value of bulk Ni ($a_{Ni(111)} = 2.488$ Å). The positions (*x*, *y*, *z*-coordinates) of C atoms and intercalant as well as *z*-coordinates of the two topmost layers of the substrate from the both sides of the slab were fully relaxed until the forces were smaller than 10^{-2} eV Å^{-1}. The convergence criteria for energy was set equal to 10^{-5} eV. To recover an effective primitive cell band structure picture from the supercell band structure (if necessary), the BandUP software was employed.[60,61] The STM images were calculated using the Tersof–Hamann formalism.[62,63] The NEXAFS spectra simulations were obtained with ELSA-software[64] according to the procedure described in refs. [49, 65]. To obtain an input for the NEXAFS spectra simulations, large supercells of (6×6), (4×4), and (3×3) periodicity when studying free-standing graphene, gr/Ni(111), and gr/RE/Ni(111) systems, respectively were employed. In the case of gr/Ni(111) and gr/RE/Ni(111) the number of nickel layers was reduced to four.

Supporting Information

Supporting Information is available from the Wiley Online Library or from the author.

Acknowledgements

This work was supported by the National Natural Science Foundation of China (Grant No. 21973059). The authors appreciate the High Performance Computing Center of Shanghai University and Shanghai Engineering Research Center of Intelligent Computing System (No. 19DZ2252600) for providing the computing resources and technical support. Y.D. and E.V. thank the "ENSEMBLE3 - Centre of Excellence for Nanophotonics, Advanced Materials and Novel Crystal Growth-Based Technologies" project (GA No. MAB/2020/14) carried out within the International Research Agendas programme of the Foundation for Polish Science co-financed by the European Union under the European Regional Development Fund and the European Union's Horizon 2020 research and innovation programme Teaming for Excellence (GA. No. 857543) for support of this work. The

© 2022 The Authors. Advanced Theory and Simulations published by Wiley-VCH GmbH

North-German Supercomputing Alliance (HLRN) and the computing facilities (ZEDAT) of the Freie Universität Berlin are acknowledged for providing computer time.

Open access funding enabled and organized by Projekt DEAL.

Conflict of Interest

The authors declare no conflict of interest.

Data Availability Statement

The data that support the findings of this study are available from the corresponding author upon reasonable request.

Keywords

density functional theory calculations, electronic and magnetic properties, graphene–metal interfaces, near-edge X-ray absorption fine structure spectra simulations

Received: December 21, 2021
Revised: March 6, 2022
Published online: April 30, 2022

[1] A. K. Geim, K. S. Novoselov, *Nat. Mater.* **2007**, *6*, 183.
[2] A. H. C. Neto, F. Guinea, N. M. R. Peres, K. S. Novoselov, A. K. Geim, *Rev. Mod. Phys.* **2009**, *81*, 109.
[3] S. D. Sarma, S. Adam, E. H. Hwang, E. Rossi, *Rev. Mod. Phys.* **2011**, *83*, 407.
[4] Y. Dedkov, E. Voloshina, *J. Phys.: Condens. Matter* **2015**, *27*, 303002.
[5] M. Yang, Y. Liu, T. Fan, D. Zhang, *Prog. Mater. Sci.* **2020**, *110*, 100652.
[6] Y. Dedkov, E. Voloshina, *Nanoscale* **2020**, *12*, 11416.
[7] M. Weser, Y. Rehder, K. Horn, M. Sicot, M. Fonin, A. B. Preobrajenski, E. N. Voloshina, E. Goering, Y. S. Dedkov, *Appl. Phys. Lett.* **2010**, *96*, 012504.
[8] M. Weser, E. N. Voloshina, K. Horn, Y. S. Dedkov, *Phys. Chem. Chem. Phys.* **2011**, *13*, 7534.
[9] Y. S. Dedkov, M. Fonin, *New J. Phys.* **2010**, *12*, 125004.
[10] D. Marchenko, A. Varykhalov, J. Sánchez-Barriga, O. Rader, C. Carbone, G. Bihlmayer, *Phys. Rev. B* **2015**, *91*, 235431.
[11] D. Usachov, A. Fedorov, M. M. Otrokov, A. Chikina, O. Vilkov, A. Petukhov, A. G. Rybkin, Y. M. Koroteev, E. V. Chulkov, V. K. Adamchuk, A. Grüneis, C. Laubschat, D. V. Vyalikh, *Nano Lett.* **2015**, *15*, 2396.
[12] N. Rougemaille, A. T. N'Diaye, J. Coraux, C. Vo-Van, O. Fruchart, A. K. Schmid, *Appl. Phys. Lett.* **2012**, *101*, 142403.
[13] A. D. Vu, J. Coraux, G. Chen, A. T. N'Diaye, A. K. Schmid, N. Rougemaille, *Sci. Rep.* **2016**, *6*, 24783.
[14] T. Vincent, E. Voloshina, S. Pons, S. Simon, M. Fonin, K. Wang, B. Paulus, D. Roditchev, Y. Dedkov, S. Vlaic, *J. Phys. Chem. Lett.* **2020**, *11*, 1594.
[15] T. E. Weller, M. Ellerby, S. S. Saxena, R. P. Smith, N. T. Skipper, *Nat. Phys.* **2005**, *1*, 39.
[16] I. I. Mazin, *Phys. Rev. Lett.* **2005**, *95*, 227001.
[17] I. I. Mazin, S. L. Molodtsov, *Phys. Rev. B* **2005**, *72*, 172504.
[18] J. Chapman, Y. Su, C. A. Howard, D. Kundys, A. N. Grigorenko, F. Guinea, A. K. Geim, I. V. Grigorieva, R. R. Nair, *Sci. Rep.* **2016**, *6*, 23254.
[19] S. Ichinokura, K. Sugawara, A. Takayama, T. Takahashi, S. Hasegawa, *ACS Nano* **2016**, *10*, 2761.
[20] J. L. McChesney, A. Bostwick, T. Ohta, T. Seyller, K. Horn, J. González, E. Rotenberg, *Phys. Rev. Lett.* **2010**, *104*, 136803.
[21] C. Hwang, D. Y. Kim, D. A. Siegel, K. T. Chan, J. Noffsinger, A. V. Fedorov, M. L. Cohen, B. Johansson, J. B. Neaton, A. Lanzara, *Phys. Rev. B* **2014**, *90*, 115417.
[22] A. V. Fedorov, N. I. Verbitskiy, D. Haberer, C. Struzzi, L. Petaccia, D. Usachov, O. Y. Vilkov, D. V. Vyalikh, J. Fink, M. Knupfer, B. Büchner, A. Grüneis, *Nat. Commun.* **2014**, *5*, 3257.
[23] P. Rosenzweig, H. Karakachian, S. Link, K. Küster, U. Starke, *Phys. Rev. B* **2019**, *100*, 035445.
[24] P. Rosenzweig, H. Karakachian, D. Marchenko, K. Küster, U. Starke, *Phys. Rev. Lett.* **2020**, *125*, 176403.
[25] A. Shikin, D. Farias, V. Adamchuk, K.-H. Rieder, *Surf. Sci.* **1999**, *424*, 155.
[26] D. Farias, K. Rieder, A. Shikin, V. Adamchuk, T. Tanaka, C. Oshima, *Surf. Sci.* **2000**, *454*, 437.
[27] A. M. Shikin, M. V. Poigin, Y. S. Dedkov, S. L. Molodtsov, V. K. Adamchuk, *Phys. Solid State* **2000**, *42*, 1170.
[28] S. Schumacher, T. O. Wehling, P. Lazić, S. Runte, D. F. Förster, C. Busse, M. Petrović, M. Kralj, S. Blügel, N. Atodiresei, V. Caciuc, T. Michely, *Nano Lett.* **2013**, *13*, 5013.
[29] S. Watcharinyanon, L. I. Johansson, C. Xia, J. I. Flege, A. Meyer, J. Falta, C. Virojanadara, *Graphene* **2013**, *2013*, 66.
[30] E. N. Voloshina, Y. S. Dedkov, *Z. Naturforsch. A* **2014**, *69*, 297.
[31] M. Kim, M. C. Tringides, M. T. Hershberger, S. Chen, M. Hupalo, P. A. Thiel, C.-Z. Wang, K.-M. Ho, *Carbon* **2017**, *123*, 93.
[32] Y. Gamo, A. Nagashima, M. Wakabayashi, M. Terai, C. Oshima, *Surf. Sci.* **1997**, *374*, 61.
[33] G. Bertoni, L. Calmels, A. Altibelli, V. Serin, *Phys. Rev. B* **2005**, *71*, 075402.
[34] D. E. Parreiras, E. A. Soares, G. J. P. Abreu, T. E. P. Bueno, W. P. Fernandes, V. E. d. Carvalho, S. S. Carara, H. Chacham, R. Paniago, *Phys. Rev. B* **2014**, *90*, 155454.
[35] A. Dahal, M. Batzill, *Nanoscale* **2014**, *6*, 2548.
[36] Y. Matsumoto, S. Entani, A. Koide, M. Ohtomo, P. V. Avramov, H. Naramoto, K. Amemiya, T. Fujikawa, S. Sakai, *J. Mater. Chem. C* **2013**, *1*, 5533.
[37] S. L. Molodtsov, C. Laubschat, M. Richter, T. Gantz, A. M. Shikin, *Phys. Rev. B* **1996**, *53*, 16621.
[38] A. M. Shikin, V. K. Adamchuk, S. Siebentritt, K. H. Rieder, S. L. Molodtsov, C. Laubschat, *Phys. Rev. B* **2000**, *61*, 7752.
[39] S. L. Molodtsov, F. Schiller, S. Danzenbächer, M. Richter, J. Avila, C. Laubschat, M. C. Asensio, *Phys. Rev. B* **2003**, *67*, 115105.
[40] E. N. Voloshina, Y. S. Dedkov, *Mater. Res. Express* **2014**, *1*, 035603.
[41] E. Voloshina, Y. Dedkov, *Phys. Chem. Chem. Phys.* **2012**, *14*, 13502.
[42] O. Eriksson, B. Johansson, R. C. Albers, A. M. Boring, M. S. S. Brooks, *Phys. Rev. B* **1990**, *42*, 2707.
[43] L. V. Dzemiantsova, M. Karolak, F. Lofink, A. Kubetzka, B. Sachs, K. v. Bergmann, S. Hankemeier, T. O. Wehling, R. Frömter, H. P. Oepen, A. I. Lichtenstein, R. Wiesendanger, *Phys. Rev. B* **2011**, *84*, 205431.
[44] P. Jacobson, B. Stoeger, A. Garhofer, G. S. Parkinson, M. Schmid, R. Caudillo, F. Mittendorfer, J. Redinger, U. Diebold, *J. Phys. Chem. Lett.* **2012**, *3*, 136.
[45] Y. Dedkov, W. Klesse, A. Becker, F. Späth, C. Papp, E. Voloshina, *Carbon* **2017**, *121*, 10.
[46] G. Prudnikova, A. Vjatkin, A. Ermakov, A. Shikin, V. Adamchuk, *J. Electron pectrosc. Relat. Phenom.* **1994**, *68*, 427.
[47] P. A. Brühwiler, A. J. Maxwell, C. Puglia, A. Nilsson, S. Andersson, N. Mårtensson, *Phys. Rev. Lett.* **1995**, *74*, 614.
[48] O. Wessely, M. I. Katsnelson, O. Eriksson, *Phys. Rev. Lett.* **2005**, *94*, 167401.
[49] E. Voloshina, R. Ovcharenko, A. Shulakov, Y. Dedkov, *J. Chem. Phys.* **2013**, *138*, 154706.

© 2022 The Authors. Advanced Theory and Simulations published by Wiley-VCH GmbH

[50] Y. Zhou, R. Ovcharenko, B. Paulus, Y. Dedkov, E. Voloshina, *Adv. Theory Simul.* **2021**, *5*, 2100319.
[51] A. Shikin, S. Gorovikov, V. Adamchuk, S. Molodtsov, P. Engelmann, C. Laubschat, *J. Electron Spectrosc. Relat. Phenom.* **1999**, *105*, 85.
[52] G. Kresse, J. Hafner, *Phys. Rev. B* **1993**, *47*, 558.
[53] G. Kresse, J. Hafner, *J. Phys. Condens. Matter* **1994**, *6*, 8245.
[54] G. Kresse, J. Furthmüller, *Comp. Mater. Sci.* **1996**, *6*, 15.
[55] J. P. Perdew, K. Burke, M. Ernzerhof, *Phys. Rev. Lett.* **1996**, *77*, 3865.
[56] P. E. Blöchl, *Phys. Rev. B* **1994**, *50*, 17953.
[57] P. E. Blöchl, O. Jepsen, O. K. Andersen, *Phys. Rev. B* **1994**, *49*, 16223.
[58] S. Grimme, J. Antony, S. Ehrlich, H. Krieg, *J. Chem. Phys.* **2010**, *132*, 154104.
[59] A. I. Liechtenstein, V. I. Anisimov, J. Zaanen, *Phys. Rev. B* **1995**, *52*, R5467.
[60] P. V. C. Medeiros, S. Stafström, J. Björk, *Phys. Rev. B* **2014**, *89*, 041407.
[61] P. V. C. Medeiros, S. S. Tsirkin, S. Stafström, J. Björk, *Phys. Rev. B* **2015**, *91*, 041116.
[62] J. Tersoff, D. R. Hamann, *Phys. Rev. B* **1985**, *31*, 805.
[63] W. A. Hofer, A. S. Foster, A. L. Shluger, *Rev. Mod. Phys.* **2003**, *75*, 1287.
[64] ELSA software, https://matcaten.com/elsa (accessed: March 2022).
[65] R. E. Ovcharenko, I. I. Tupitsyn, E. P. Savinov, E. N. Voloshina, B. Paulus, Y. S. Dedkov, A. S. Shulakov, *Phys. Chem. Chem. Phys.* **2013**, *15*, 6749.

© 2022 The Authors. Advanced Theory and Simulations published by Wiley-VCH GmbH